Int. J. Therm. Sci. (2001) 40, 539–549

S1290-0729(01)01242-X/FLA

Effects of multiple scattering and reflective boundary on the transient radiative transfer process

Pei-feng Hsu

Mechanical and Aerospace Engineering Department, Florida Institute of Technology, Melbourne, FL 32901, USA

(Received 5 April 2000, accepted 28 August 2000)

Abstract — A time-dependent Monte Carlo method is developed for modeling the transient radiative transfer within absorbing and scattering media. It is well known that the transmitted and reflected signal from a short-pulse incident radiation to the scattering medium has very long, extended temporal spread. However, two important but yet to be clarified issues are: (1) the relative and combined influences of the multiple scattering and reflective boundary on the transient radiative transfer process; and (2) the effect of the incident temporal pulse width and pulse shape on the radiative transport. It is found that the pulse width and shape has little effect on the transient radiative transport process when the pulse temporal width is much smaller than the pulse transmission time through the one-dimensional slab. The stochastic simulation of time-of-flight of photon compares very well with the results obtained by a recently developed Volterra integral equation formulation of the transient radiative transfer. © 2001 Éditions scientifiques et médicales Elsevier SAS

transient radiative transfer / Monte Carlo method / numerical solutions / reflective surface / scattering medium

Nomenclature

a	absorption coefficient	m^{-1}
c	propagation speed of radiation transport in the medium	$m{\cdot}s^{-1}$
d	distance	m
G	incident radiation or integrated intensity	$W{\cdot}m^{-2}$
H	Heaviside unit step function	
I	radiation intensity	$W{\cdot}m^{-2}{\cdot}sr^{-1}$
I_0	radiation intensity at boundary $z = 0$	$W{\cdot}m^{-2}{\cdot}sr^{-1}$
j	volume element index	
$\hat{k}$	unit vector in the z-direction	
q	radiative flux	$W{\cdot}m^{-2}$
R	random number	
s	geometric path length	m
$\hat{s}$	unit vector along a given direction	
t	time	s
z	axial coordinate	m
z_0	medium thickness	m

Greek symbols

δ	a small number or the Dirac delta function	
ζ	dimensionless position or optical coordinate $= \kappa z$	
η	dimensionless time $= \kappa c t$	
κ	extinction coefficient $= a + \sigma$	m^{-1}
μ	direction cosine	
ρ	surface reflectivity	
σ	scattering coefficient	m^{-1}
τ	optical thickness of the medium $= \kappa z_0$	
Φ	scattering phase function	
Ω	solid angle	sr
ω	scattering albedo $= \sigma/\kappa$	

E-mail address: phsu@fit.edu (P.-f. Hsu).

1. INTRODUCTION

The interests of transient radiative transfer have been found in, for example, the study of light interaction in living tissues [1], in microscale systems [2], pulsed laser interaction with materials [3, 4]. Flock et al. [5] used Monte Carlo (MC) method to study the fluence (the time-integrated incident radiation) distribution. However, they did not provide transient results for direct comparison. Hasegawa et al. [6] used MC method to simulate the transient light transmission through the living tissue which was characterized by strong forward scattering

phase function. The transient radiation transport inside the medium was not presented and apparently not needed for comparison with the measured reflected and transmitted signals from the samples. The input radiation was assumed to be an infinitesimal (a Dirac delta) pulse with zero temporal width, i.e., all the photons were emitted at the same time. This assumption would have induced error in the short time response of temporal transmittance signal. Their results at larger time were correct as similar results were obtained in this study and, as will be shown later, the temporal width of the pulse has little effect on the long time transient response. Nevertheless, the approximation can be avoided by simulating the emission of each energy bundle at discrete time within a given finite time interval. Their MC solutions were subjected to statistical fluctuations due to low bundle numbers in the transmitted signal of optically thick sample. Similar situation was encountered in this study but minimized to the extent that can be handled by the amount of computer main memory. The beam size and detector size effect was considered in their work but not in this study where plane wave of incident radiation is assumed.

To gain a detailed knowledge of the pulse shape and width effect, it is important to represent the real physics as close as possible in the simulation. Furthermore, the effect of pulse shape and width depend on the relative magnitude of the wave propagation distance (ct_p) within the time scale of the pulse width (t_p) and the slab thickness (L), i.e., $t^* = ct_p/L$. In the cases examined in this study, the ratio is quite low ($t^* < 0.05$) and it is expected that the pulse width effect on the long time transmittance and reflectance is thus insignificant compared with the case when this ratio is large ($t^* \approx 1$). Recently Wu [7] examined the pulse propagation within scattering media with the condition of $t^* \approx 1$, although his work is not explicitly about the pulse shape/width effect. He used an exact integral formulation to simulate the transient radiative transport.

Brewster and Yamada [8] later conducted the transient study using the same MC algorithm used by Hasegawa et al. [6] which, in turn, was based on the work of Wilson and Adam [9]. They examined various effects, i.e., albedo, optical thickness, anisotropic scattering, and the detector size, on the reflected and transmitted temporal signals. The results agreed well with the diffusion approximation in the long time time-resolved signals from optically thick media.

Rackmil and Buckius [10] used an adding-doubling technique to study the transformed transient radiative transfer equation. Their results did not include the optically thick medium which is typical in living tissues. The solution technique is difficult to extend to multidimensional media and this limits its applicability in complex geometry problems.

In a detailed review of the various models of the transient radiative transfer by Mitra and Kumar [11] it was reported that the scattered, reflected and transmitted signals possess the multiple scattering induced temporal signature that persists for time periods greater than the duration of the source pulse and is a function of the source pulse width, the scattering and absorbing properties of the medium, and the location in the medium where the properties undergo changes. This variation of the signal with time is an additional parameter to gain radiative property information of the participating medium. Ishimaru [12] discussed the pulse wave transport within the random distribution of scattering particles.

Much of the attention of the prior investigations focused on the light interactions with the tissues which are characterized by large extinction coefficient and very high scattering albedo ($\omega \sim 1$). It is interesting to know whether similar laser pulse interactions within intermediate optical thickness materials can be found as in the optically dense tissues. The MC algorithm used in this work, even though only the isotropic scattering phase function was considered, can examine the highly forward scattering if the effective absorption and scattering coefficients are used instead [13]. Nevertheless, implementing an anisotropic scattering phase function is rather straightforward with the Monte Carlo method. Since most existing work only deals with optically thick media within which the intensity distribution behaves diffusely, an isotropic scattering phase function should adequately describe the scattering phenomena in such media without loss of fidelity.

An important issue of pulse transport inside the medium is the relative influence of the multiple scattering and reflective boundaries. In the existing literature, only a few studies have considered the reflective boundary effect (for example, Aronson [14], Pomraning and Ganapol [15], Zhu et al. [16]). However, these are based on the diffusion approximation. The temporal spread of the output signals was generally considered to be caused by the multiple scattering only. If the boundary surface is reflective, then the multiple reflections and partial transmissions at the surfaces may also contribute to the temporal spread. Since the participating media of interest typically have a refractive index greater than one, surface reflection is bound to occur [15]. Considering a multidimensional geometry with a fraction of its boundary being reflective, the temporal spread of the output signals will be complicated by the reflection and cannot be ad-

equately described by the multiple scattering alone. Because no existing model has treated the reflective surface accurately, the exact quantification of its influence is still needed. To avoid the unnecessary complexities, this study will only consider one-dimensional geometry with both boundaries having equal specular reflectivity.

The motivation of the current study is to gain a fundamental understanding the unique features of transient radiation (especially with the short pulse as the incident source) and its interaction with the participating medium. In the prior MC simulations of the transient processes, direct comparisons with the exact solutions were not available. In fact, all these transient MC simulations implicitly assumed that the MC results were accurate within the statistical error. However, it has been known that different implementations of the MC technique could lead to large difference in the solutions for the same problem [18]. The rigorous verification is therefore needed, even for the Monte Carlo method. A recently developed Volterra integral equation formulation of the transient radiation by the author [19] provides high order accuracy solutions which were used to compare and verify the current implementation of the Monte Carlo algorithm.

2. A MONTE CARLO ALGORITHM OF THE TRANSIENT RADIATIVE TRANSFER

The transient radiative transfer of the radiative intensity in direction $\hat{s}$ is given by [17, 20, 21]

$$\frac{\partial I(z,\hat{s},t)}{c\partial t}+\frac{\partial I(z,\hat{s},t)}{\partial z} = -\kappa I(z,\hat{s},t)+\frac{\sigma}{4\pi}\int_{\Omega'=4\pi} I\left(z,\hat{s}',t\right)\Phi\left(\hat{s}',\hat{s}\right)\mathrm{d}\Omega' \tag{1}$$

The transport equation is an integro-differential type. The left-hand side is the hyperbolic wave equation. The emission term on the right-hand side is not considered as the medium under consideration is cold and its temperature distribution is not affected by the small amount of incident radiation energy. It is further assumed that the radiative properties of the medium and boundary remain unchanged during the transient process. The analytical solution of equation (1) is difficult to obtain. Recently, Tan and Hsu [19] derived an integral formulation of the transport equation. The resulting Volterra integral equation can be solved with many existing quadrature schemes. The integral formulation avoids the difficulty encountered by the differential treatment when dealing with the collimated incident radiation, i.e., the discontinuity at the wave front [22]. In this study, a stochastic approach using the Monte Carlo method is adopted to solve equation (1).

The Monte Carlo algorithm implemented in this study is based on the work by Fleck [23] with modifications to improve the computational efficiency and extensions to handle reflective boundaries and collimated incident radiation. Only the salient features are described herein. In-depth discussion of the algorithm can be found in Fleck [23] and Siegel and Howell [17]. The problem under consideration is the transient radiative transfer within a one-dimensional absorbing and scattering slab with either transparent or specularly reflective boundaries. The incident plane wave can be a temporal step function, a square pulse, or a Gaussian pulse with finite temporal width. The incidence can be diffusive or collimated.

In the MC algorithm each energy bundle's local position, time, and travel direction are recorded. Detailed information of incident intensity and radiative flux distribution and history are maintained. This will provide more physical insights than only calculating the transmittance and reflectance and also allows the coupling with the energy equation if necessary.

2.1. External radiation

The external radiation applied at $z = 0$ will enter into the medium and start the emission of energy bundles. For all cases considered in this study, the incident radiation source is unpolarized and incoherent. For reflective boundary, the energy emitted at $z = 0$ will equal the portion of external radiation that is refracted into the medium. At the nth time step, the energy bundle starts its trajectory at the location and time of

$$z = 0 + \delta \tag{2}$$

and

$$t = (n - 1 + R_t)\Delta t \tag{3}$$

where δ is a small number and R is the random number. The subscript associated with R distinguishes different random number. Equation (3) allows the energy bundles to emit uniformly in a given time step and each bundle is emitted at different time. Depending on the externally applied radiation is diffuse or collimated, the bundle will start the trajectory at a direction (μ) determined by the cumulative distribution function [17].

2.2. Energy bundle trajectory

At the current position and time (z, t) of each bundle, three distances are calculated:

$$d_b = \begin{cases} \dfrac{(j+1)\Delta z - z}{\mu}, & \text{if } \mu \geq 0 \\ \dfrac{z - j\Delta z}{-\mu}, & \text{if } \mu < 0 \end{cases} \tag{4}$$

$$d_s = -\frac{\ln R_d}{\kappa} \tag{5}$$

$$d_c = c\big[(n+1)\Delta t - t\big] \tag{6}$$

d_b is the distance to the nearest mesh boundary. The j index in equation (4) is the volume element where the bundle is located. d_s is the distance to the next particle interaction event which may be scattering or absorption. d_c is the distance to census time, i.e., the distance that the bundle will travel until it reaches the next time step. All three distances are positive. After these are calculated, the shortest distance is chosen to follow. Physically, the shortest distance means the event will occur before the other two. Since many repetitive calculations of the distances are required, the algorithm needs to have some check mechanisms to avoid division by zero. These additional mechanisms take up computational time. After each event, the position, time, and location of the energy bundle are updated [23].

To tally the energy bundles that reach the next time step (i.e., when d_c is the smallest distance) before any particle interactions, the information of these bundles (position, travel time, direction) has to be stored and used as the starting points at the next time step. These bundles are called the census (or accumulated) bundles. At the beginning of each time step the census bundles, if there is any, are first treated and then the emission of new bundles. The amount of memory needed for tracking the bundles is three two-dimensional arrays with each corresponding to the position, time, and direction of the census bundles. Each array has the first dimension be large enough to accommodate the maximum number of census bundles, which is set to be 10^7. This dimension is limited by the computer system memory. The second dimension is 2 as only two successive time steps are required for tallying purpose. Due to the census arrays used, the memory requirement is quite high as compared with the steady state algorithm or other transient MC algorithm where the transport process within the medium is not of interest, e.g., Brewster and Yamada [8] and Hasegawa et al. [6]. In the latter case only the transmitted and reflected bundles were recorded. If the detailed record of bundles' travel history within the medium is not needed then the memory requirement will be much lower.

The calculation of d_b is not needed if the medium is homogeneous, i.e., uniform radiative properties. For nonhomogeneous medium the property distribution is assumed to be piecewise constant within each volume element. For every mesh boundary crossing (when d_b is the smallest) the following adjustment is made:

$$d_s' = (d_s - d_b)\frac{\kappa_j}{\kappa_j'} \tag{7}$$

where κ_j' is the extinction coefficient of the next volume element.

At each time step, two functions are calculated based on the census bundles' information. First, $G(z,t)$ is the incident radiation or direction-integrated intensity defined as

$$G(z,t) = \int_{4\pi} I(z, \hat{s}, t)\, \mathrm{d}\Omega \tag{8}$$

and $q(z,t)$ is the full-range radiative heat flux,

$$q(z,t) = \int_{4\pi} I(z, \hat{s}, t) \cos(\hat{s}, \hat{k})\, \mathrm{d}\Omega \tag{9}$$

The G and q functions are integrated at each time step for all volume elements to obtain their temporal and spatial distributions. The G function at each time step is obtained by tallying the number of energy bundles falling into each volume element and multiplying the energy per bundle. The q function integral is performed similarly except the additional multiplication with the cosine. Since in many situations the q responses are very similar to those of G and for brevity, only the G results are presented for discussion. In all calculations, the intensity of the external radiation is normalized to one. The position z is normalized to $\zeta = \kappa z$. The time t is normalized to $\eta = \kappa c t$. The optical thickness of the medium is $\tau = \kappa z_0$. For one time step $(\Delta\eta)$, the radiation wave front travels one mesh size distance $(\Delta\zeta)$.

3. RESULTS AND DISCUSSION

3.1. Verification of Monte Carlo solution

To verify the Monte Carlo algorithm used in this study, the results of cases 1, 2, and 3 (see definitions in *table I*) are compared with the same cases in Tan and Hsu [19] in which accurate transient solutions were obtained. These

TABLE I
Boundary and physical conditions of verification cases.

Case	Boundary 1 $z=0$	Medium property	Boundary 2 $z=z_0$
1	diffuse emission $I(0,\hat{s},t)=I_0H(t)$ $\rho=0$	homogeneous $\tau=1,\ \omega=0.5$	non-reflection $\rho=0$
2	diffuse emission $I(0,\hat{s},t)=I_0H(t)$ $\rho=0$	homogeneous $\tau=1,\ \omega=0.5$	specular reflection $\rho=1$
3	collimated radiation $I(0,\hat{s},t)$ $=I_0H(t)\delta(1-\hat{s}\cdot\hat{k})$ $\rho=0$	homogeneous $\tau=1,\ \omega=0.5$	non-reflection $\rho=0$

TABLE II
RMS error of the Monte Carlo solutions of case 1.

Energy bundle number per time step	RMS error of $G(z/z_0=0.005,t)$	RMS error of $q(z/z_0=0.005,t)$
$1{\cdot}10^4$	$4.4{\cdot}10^{-3}$	$9.1{\cdot}10^{-3}$
$3{\cdot}10^4$	$2.6{\cdot}10^{-3}$	$3.3{\cdot}10^{-3}$
$5{\cdot}10^4$	$2.5{\cdot}10^{-3}$	$2.7{\cdot}10^{-3}$
$7{\cdot}10^4$	$2.0{\cdot}10^{-3}$	$2.3{\cdot}10^{-3}$

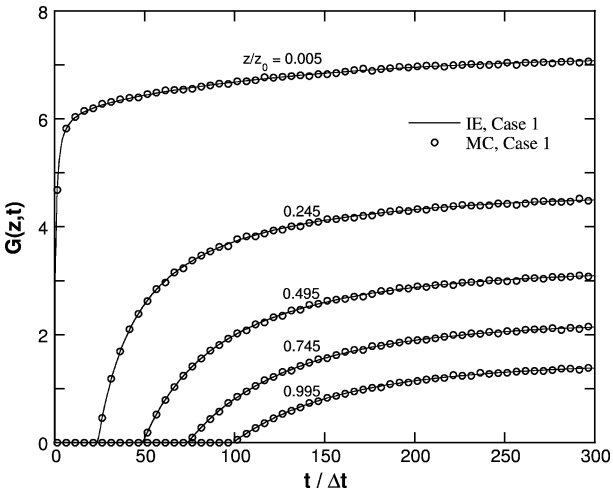

Figure 1. Incident radiation as a function of time at different location (case 1).

cases have the Heaviside unit step function as the transient input at the boundary $z=0$ with normalized incident diffuse or collimated intensity equal to 1. A rigorous test of the number of energy bundles needed in each time step of case 1 is shown in *table II*. For the step function boundary condition, it was determined that $3{\cdot}10^4$ energy bundles per time step was the best compromise among the accuracy, memory, and computational time requirements. It should be noted that using $7{\cdot}10^4$ boundary emission bundles per time step the number of the census bundles at later time steps could reach as high as 10^7 and it takes about 3 hours to complete a simulation. Because of tallying the bundle's travel history at successive time steps inside the medium as described above, the memory requirement was quite high — about 250 MB with $7{\cdot}10^4$ bundles per time step. All calculations were conducted on a 633 MHz 21164A Alpha processor PC. *Table II* demonstrates the consistence of the MC algorithm. Similar root-mean-square (RMS) error trend was also observed for the cases of reflective boundary (case 2) and collimated incidence (case 3). *Figures 1–3* show the good agreement

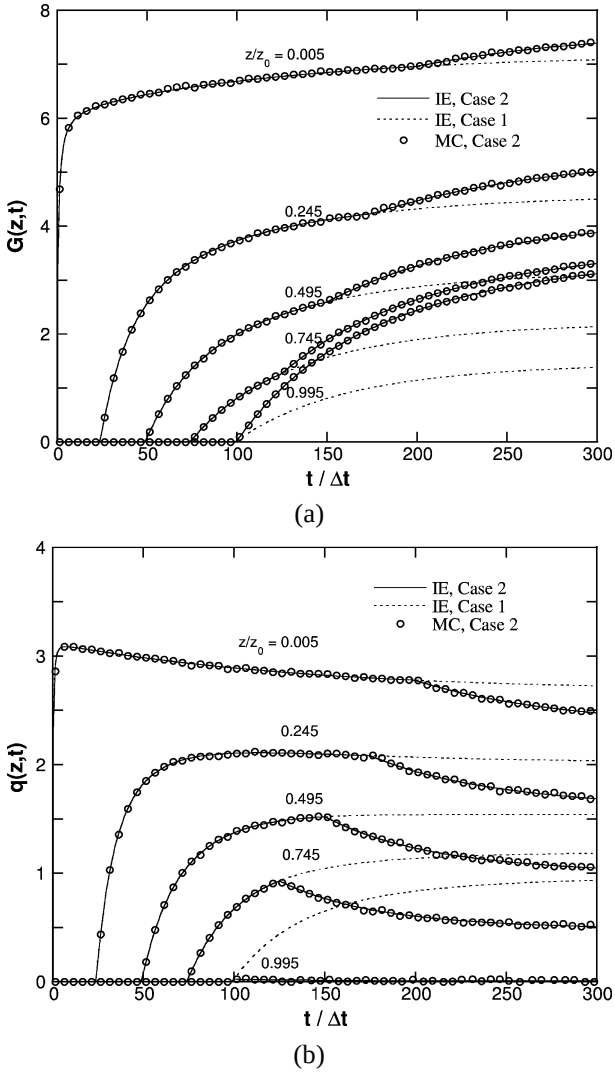

Figure 2. (a) Incident radiation as a function of time at different location (cases 1 and 2). (b) Radiative flux as a function of time at different location (cases 1 and 2).

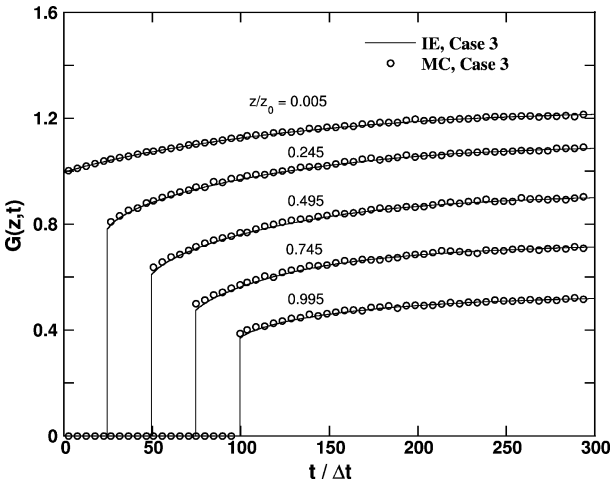

Figure 3. Incident radiation as a function of time at different locations (case 3).

between the MC solutions and the integral equation solutions. Detailed discussion of the wave characteristics and the integral equation formulation are given in Tan and Hsu [19]. The verifications of the three cases ensure MC solutions of all different boundary conditions (diffuse and collimated external radiation, and reflective surface) are correct.

3.2. Scattering albedo

The influence of scattering albedo is examined in two optical thicknesses.

3.2.1. Intermediate optical thickness

In *figure 4*, with $\tau = 1$ and transparent (or cold black) boundaries, the effect of scattering albedo strongly dominates the time response right after the pulse. Larger albedo increases the G values at both long time, *figure 4(a)*, and short time responses, *figure 4(b)*. Similar trends are observed in the radiative flux responses but not shown for brevity. Large albedo promotes stronger multiple scattering interactions of photons with the participating medium and, hence, produces stronger tail behind the pulse.

The calculation starts from $t/\Delta t = 0$ and continues up to $t/\Delta t = 500$ but only $t/\Delta t = 0$ to 300 is shown in *figure 4*. For the given conditions and at $t/\Delta t = 300$ the transient response curves have the similar "asymptotic log slope" described by Brewster and Yamada [8], i.e., the time resolved curves of transmittance and reflectance have slope equal $(1 - \omega_I)$ which is based on

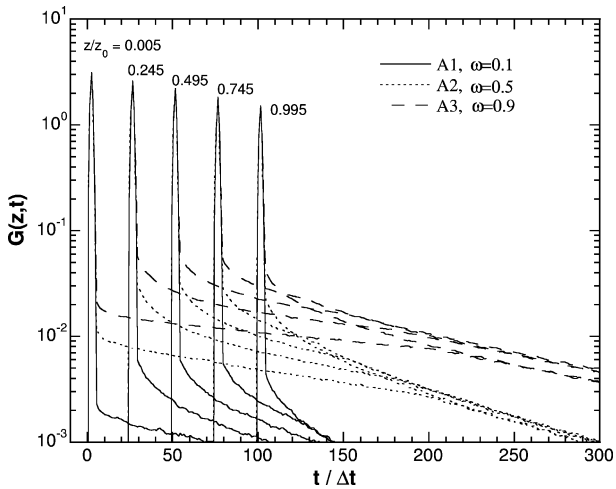

(a)

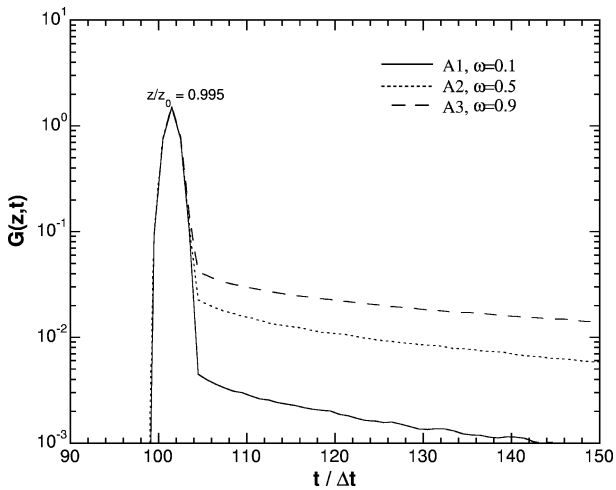

(b)

Figure 4. Effect of scattering albedo. Cases A1, A2, and A3 have $\rho = 0$, $\tau = 1$, and Gaussian pulse incidence. (a) Effect of scattering albedo on the time response curve of incident radiation inside the medium of intermediate optical thickness. (b) The temporal response of G at $z/z_0 = 0.995$ before the pulse exiting the medium.

diffusion approximation. ω_I is an effective isotropic scattering albedo to account for the anisotropic scattering effect. Although the slope of the time response curve of G varies with different albedo but to a lesser degree than the reflectance curve of a semi-infinite slab with large optical thickness described in Brewster and Yamada [8]. It is found that the simple relation above to predict the log slope is not applicable in the intermediate optical thickness. At long time close to steady state the G distribution inside the medium becomes symmetric with respect to the mid-plane of the slab as shown in the case A3 curves

TABLE III
Physical conditions of test cases with temporal-Gaussian collimated incidence.

Case	Albedo, ω	Surface reflectivity, ρ	Optical thickness, τ	Pulse shape and width
A1	0.1	0	1	Gaussian, $5\Delta\eta$
A2	0.5	0	1	Gaussian, $5\Delta\eta$
A3	0.9	0	1	Gaussian, $5\Delta\eta$
A4	0.9	0.5	1	Gaussian, $5\Delta\eta$
A5	0.9	0.9	1	Gaussian, $5\Delta\eta$
B1	0.9	0	0.1	Gaussian, $5\Delta\eta$
B2	0.9	0	15	Gaussian, $5\Delta\eta$
B3	0.9	0	30	Gaussian, $5\Delta\eta$
B4	0.998	0	30	Gaussian, $5\Delta\eta$
B5	1	0	10	Gaussian, $5\Delta\eta$
C1	1	0	10	square, $\Delta\eta$
C2	0.9	0	10	square, $\Delta\eta$
C3	1	0.9	10	square, $\Delta\eta$
C4	1	0.5	10	square, $\Delta\eta$

of *figure 4(a)*. This indicates the transmittance and reflectance values at long time are equal. *Figure 4(b)* shows that larger scattering albedo increases the after-pulse G values. The multiple scattering has the dominant effect of the temporal response.

3.2.2. Large optical thickness

The study of large optical thickness is of interest since the living tissues have large scattering coefficient. For a typical sample size of several centimeter thickness, the optical thickness could be in the order of 10 or greater. To simulate the multiple scattering in such media, only large albedo was considered and the results are given in *figure 5*. It is evident that at large optical thickness, a moderate increase of ω from 0.9 (a very large albedo already) to 0.998 can cause significant increase in the transient response of G function. With albedo close to 1, there is little loss of energy bundles due to the absorption. Most of the loss is caused by the bundles scattered out of the slab. In addition, for both cases B3 and B4 very significant multiple scattering causes the temporal signal at large z positions to increase with the time and reach a peak value at long time (see B3 curve at $z/z_0 = 0.495$). The large albedo in optically thick media will keep more photons inside the materials and take longer to reach steady state, i.e., the temporal spread of the signal after the pulse passes through the medium will be larger.

Due to the low signal level, the B3 curve at $z/z_0 = 0.995$ is not shown in *figure 5*. This is because very few bundles can pass through the optically thick medium,

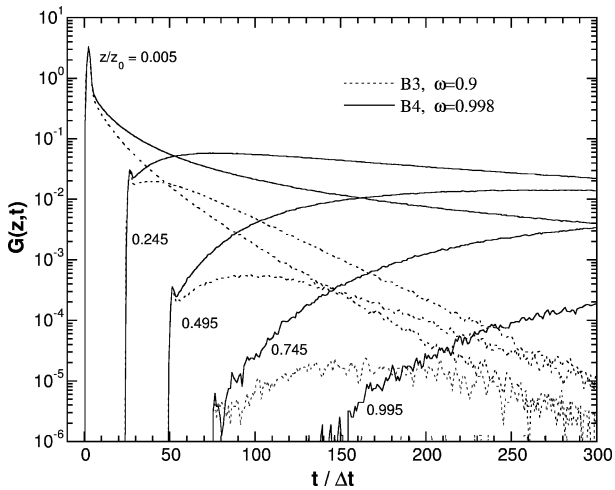

Figure 5. Effect of scattering albedo on the time response curve of incident radiation inside the medium of large optical thickness. Cases B3 and B4 have $\rho = 0$, $\tau = 30$, and Gaussian pulse incidence.

which has some amount of absorption. Furthermore, very significant fluctuations are observed in the B3 curve at $z/z_0 = 0.745$ as well as the long time responses at smaller z positions. Such fluctuations were also found in other MC simulations, e.g., Hasegawa et al. [6] and Brewster and Yamada [8]. The remedy is to increase the number of energy bundles at the emission. This was not possible in this study as the memory storage for census bundles arrays had reached the system memory limit of 256 MB RAM. For the pulsed radiation input, the total number of emission energy bundles used in

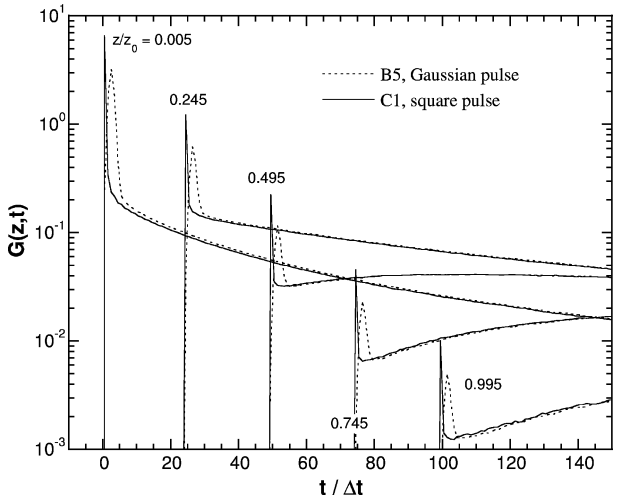

Figure 6. Effect of pulse width and shape. Cases B5 and C1 have $\rho = 0$, $\tau = 10$, and $\omega = 1$.

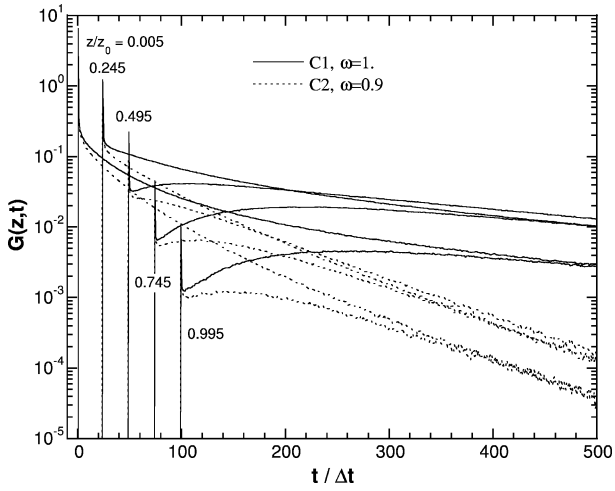

Figure 7. Effect of scattering albedo on the time response curve of incident radiation inside the medium of large optical thickness. Cases C1 and C2 have $\rho = 0$, $\tau = 10$, and square pulse incidence.

the simulation was about 10^7 and the number of census bundles is close to this number for large ω and τ medium. Nevertheless, even with the fluctuations the MC simulation retains the main characteristics of the temporal response. An alternative is to use the reverse Monte Carlo technique to reduce the computational time and memory usage if only the solutions at specified time and location are needed.

3.3. Pulse width and shape

Two types of pulsed incidence are compared: (1) energy bundles were emitted uniformly within a square pulse that has temporal width of 1 time step; and (2) a Gaussian pulse with pulse width of 5 time steps. The square wave is formed by two sequential Heaviside unit step functions. Equal amount of energy and approximately the same total number (10^7) of energy bundles are emitted in either pulse. In *figure 6* very little effect, except the short time response right after the pulse, can be seen in the G distribution for two different pulse widths and pulse shapes. The long time response is not shown in the figure since the two cases (B5 and C1) are nearly identical. This is consistent with the energy balance requirement since the same amount of energy is entering the same material, any residual effect after the pulse leaves the material should be identical. The long time C1 curves are presented in *figure 7*. The pulse height of C1 is taller than that of B5 since the same amount of radiative energy is deposited in a shorter time interval ($\Delta\eta$ versus $5\Delta\eta$).

Figure 7 shows the effect of albedo at optical thickness $\tau = 10$. It has similar G distributions as shown in *figure 5* ($\tau = 30$) even though the input pulse shape and width are different. Comparing these two figures, it again confirms that the pulse shape and width have little effect on the transient transfer process. The long time responses of C1 at different z positions clearly show the symmetric distribution within the slab as the A3 curves in *figure 4(a)*. This indicates equal value of reflectance and transmittance will be measured at long time after pulse leaves the medium.

3.4. Surface reflectivity

Since the interest is to examine the transient interaction within the medium, the simulation is based on the same amount of radiative energy being deposited inside the medium. For the reflective boundary, this means more incidence energy (external to the medium) is applied to account for the reflection loss $(1 - \rho)$ at the incidence surface, i.e., $z = 0$.

To improve the model, the Fresnel reflection relation can be used. However, the main interest is to demonstrate the frequently overlooked effect of reflective surface on the photon propagation within the medium and, thus, the output radiative signatures. Using the Fresnel reflectivity, which is straightforward in the current MC algorithm, will not add much to the results.

In a transient radiative transport process, the traditional definitions of reflectance and transmittance (which

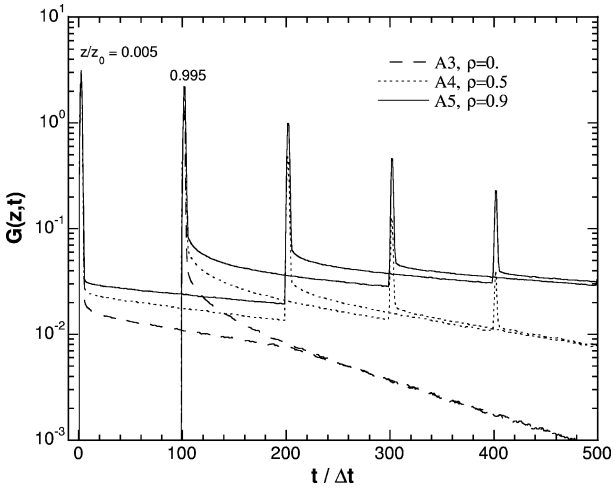

Figure 8. Effect of surface reflectivity at intermediate optical thickness. Cases A3–A5 have $\omega = 0.9$, $\tau = 1$, and Gaussian pulse incidence.

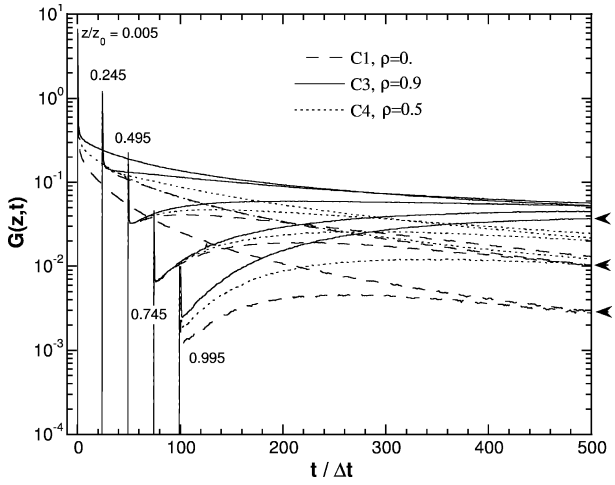

Figure 9. Effect of surface reflectivity at large optical thickness. Cases C1, C3, and C4 have $\omega = 1$, $\tau = 10$, and square pulse incidence.

are based on the ratio of output flux to input flux) may not be suitable when the incident energy is contained within a temporal pulse. This should be considered when reporting reflectance and transmittance data either from measurement or from simulation. The surface reflectivity effect is also examined in two optical thicknesses.

3.4.1. Intermediate optical thickness

Figure 8 depicts the transient responses at two z positions of $\tau = 1$. With the cold and black (or transparent) boundaries, the case A3 curves monotonically decrease to small magnitude at long time. On the other hand, when the boundaries become reflective (case A4, $\rho = 0.5$), the attenuated pulse remains inside the medium and persists for a long time. The pulse shape and width stay the same even at long time. With highly reflective boundary surfaces (case A5, $\rho = 0.9$) the pulse is basically bounced back and forth inside with little loss of energy. At long time the highly reflective surfaces of the medium will keep more residue energy than the less reflective or transparent surface. The A4 and A5 curves indicate that it takes longer time to reach steady state than the non-reflective case. Because of the distinctive pulse shape after the reflection, the information may be used to infer slab thickness and/or extinction property. It appears that the long time slope correlates to the reflectivity, i.e., larger ρ curve has smaller slope in the long time. A more extensive study is needed to find the correlation.

3.4.2. Large optical thickness

Figure 9 is the result with $\tau = 10$ and $\omega = 1$. It is interesting to note that the visible pulse shape in *figure 8* disappears in the optically thick and strong scattering medium. First, the strength of pulse is attenuated more due to larger τ. Secondly, the pulse is masked by the stronger multiple scattering effect. Therefore, the pulse is not visible. Nevertheless, the surface reflectivity effect is just as evident as the lower optical thickness case. The G distributions of C3 and C4 have not reached the symmetric profile at $t/\Delta t = 500$ as does the case C1. This indicates that for reflective boundary it takes longer time to reach steady state and the temporal spread of the transmittance signal will also last much longer.

The existing energy bundles (and thus, the reflectance and transmittance) will be affected by the surface reflectivity in either intermediate or large optical thickness media. It becomes critical in the interpretation of the measured transmittance and reflectance if the surface property is unknown. The neglect of the surface reflection will result measurement of larger reflectance and transmittance values.

3.5. Optical thickness

Brewster and Yamada [8] had examined this effect on the media with $\tau \geq 10$. For completeness, wider range of optical thickness is considered in this study. *Figure 10*

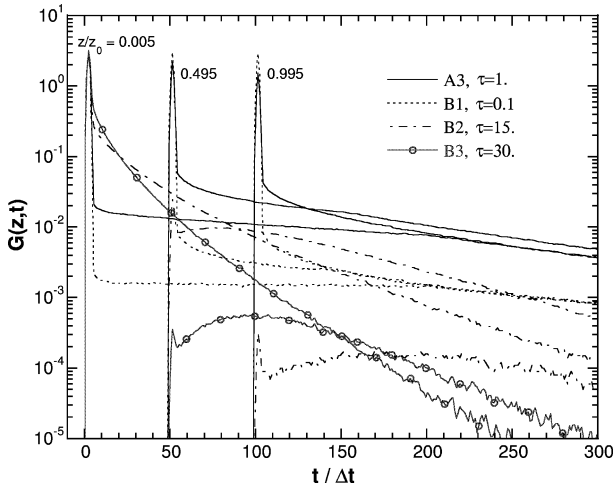

(a)

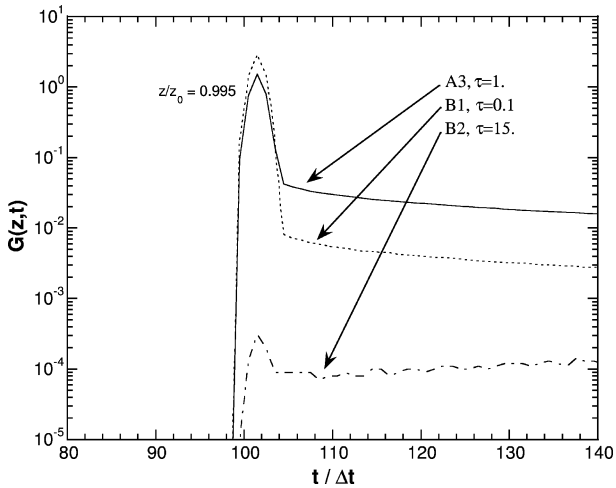

(b)

Figure 10. (a) Effect of optical thickness. The cases have $\omega = 0.9$, $\rho = 0$, and Gaussian pulse incidence. (b) Effect of optical thickness. The cases have $\omega = 0.9$, $\rho = 0$, and Gaussian pulse incidence. Only the time response curves at $z/z_0 = 0.995$ are shown.

contains the variation of optical thickness from 0.1 up to 30 with $\omega = 0.9$. The G distributions are quite different for cases with $\tau \leq 1$ and cases with $\tau \geq 10$. For the large optical thickness cases at larger z position, the G temporal distribution curves have a maximum value after the pulse (see *figure 10(a)*). The smaller optical thickness cases do not have such characteristic. This can be explained by the difference in the effect of scattering in conjunction with optical thickness. For case A3 and B1, more photons can travel through the medium with few scattering events. Therefore, the tail portion (after the pulse) of the G curve stays at relatively large value compared with cases B2 and B3. For the latter cases, most photons are being absorbed or scattered out in the small z region. For the remaining photons that do penetrate deep into the medium, they meet with strong scattering effect, which causes the peak in the tail portion of the G curve after the pulse passes through the medium. Since far fewer photons will be able to penetrate into the medium, the overall G distribution has smaller magnitude.

Figure 10(b) shows the immediate G values following the pulse at position of $z/z_0 = 0.995$. The G values at pulse peaks are attenuated exponentially according to the optical thickness. Right after the pulse, the G value of case B1 ($\tau = 0.1$) is actually less than that of case A3 ($\tau = 1$). Such behavior is contrary to the steady state measurement where the small τ medium will have less attenuation and larger transmittance signal. The larger after-pulse G value of A3 is due to the stronger scattering effect. For much larger optical thickness of B2, the overall G curve is attenuated to a much greater extent as explained above. Therefore, its G curve stays lower.

4. CONCLUSIONS

The Monte Carlo simulations are conducted for transient radiative transfer process within the absorbing, scattering, and non-emitting participating media. The results for incident intensity in the medium with different boundary conditions are presented. Various effects, including the scattering albedo, pulse shape and width, surface reflectivity, and optical thickness, are examined regarding their influences on the distribution and history of integrated intensity. It is shown that the scattering albedo is the most important factor for intermediate to large optical thickness media. For large optical thickness media, the high scattering albedo will cause a peak in the temporal response of the incident radiation function. The surface reflectivity can have significant impact on the radiative energy distribution during the transient process and needs to be considered in the interpretation of the measured reflectance and transmittance signals. For the conditions considered in this study, the pulse shape and pulse width have little influence on the transient process except the short time after the pulse. The Monte Carlo algorithm can be extended to treat the medium with non-uniform radiative property distribution and multi-dimensional geometry. Such situation is typical in many engineering applications. The simulation of the short pulse transport inside the nonhomogeneous media will be considered in the immediate future.

Acknowledgements

The author would like to thank Mrs. Danya Zhao for the assistance at the beginning of the study. The work is supported by Sandia National Lab. with contract AW-9963.

REFERENCES

[1] Yamada Y., Light–tissue interaction and optical imaging in biomedicine, in: Tien C.L. (Ed.), Annual Review of Fluid Mechanics and Heat Transfer, Vol. 6, Begell House, New York, 1995, pp. 1–59.

[2] Majumdar A., Microscale energy transport in solids, in: Tien C.L. et al. (Eds.), Microscale Energy Transport, Begell House, New York, 1998, pp. 1–93.

[3] Longtin J.P., Tien C.L., Saturable absorption during high-intensity laser heating of liquids, J. Heat Tran. 118 (1996) 924–930.

[4] Qui T.-G., Tien C.L., Short pulse laser heating in metals, Int. J. Heat Mass Tran. 35 (1992) 719–726.

[5] Flock S.T., Patterson M.S., Wilson B.C., Wyman D.R., Monte Carlo modeling of light propagation in highly scattering tissues — I: Model predictions and comparison with diffusion theory, IEEE Trans. Med. Eng. 36 (1989) 1162–1168.

[6] Hasegawa Y., Yamada Y., Tamura M., Nomura Y., Monte Carlo simulation of light transmission through living tissues, Appl. Opt. 30 (1991) 4515–4520.

[7] Wu C.-Y., Propagation of scattered radiation in a participating planar medium with pulse irradiation, J. Quant. Spectr. Rad. Transfer 64 (1999) 537–548.

[8] Brewster M.Q., Yamada Y., Optical properties of thick, turbid media from picosecond time-resolved light scattering measurements, Int. J. Heat Mass Tran. 38 (1995) 2569–2581.

[9] Wilson B.C., Adam G., A Monte Carlo model for the absorption and flux distributions of light in tissue, Med. Phys. 10 (1983) 824–830.

[10] Rackmil C.I., Buckius R.O., Numerical solution technique for the transient equation of transfer, Numer. Heat Tran. 6 (1983) 135–153.

[11] Mitra K., Kumar S., Development and comparison of models for light-pulse transport through scattering-absorbing media, Appl. Opt. 38 (1999) 188–196.

[12] Ishimaru A., Wave Propagation and Scattering in Random Media, Academic Press, New York, 1978, chapter 5, p. 93.

[13] Hsu P.-F., Tan Z., Howell J.R., Radiative transfer by the YIX method in a nonhomogeneous, scattering and non-gray medium, J. Thermophys. Heat Tran. 7 (1993) 487–495.

[14] Aronson R., Boundary conditions for diffusion light, J. Opt. Soc. Am. A 12 (1995) 2532–2539.

[15] Pomraning G.C., Ganapol B.D., Asymptotically consistent reflection boundary conditions for diffusion theory, Ann. Nucl. Energy 22 (1995) 787–817.

[16] Zhu J.X., Pine D.J., Weithz D.A., Internal reflection of diffusive light in random media, Phys. Rev. A 44 (1991) 3948–3959.

[17] Siegel R., Howell J.R., Thermal Radiative Heat Transfer, 3rd ed., McGraw-Hill, New York, 1992, chapter 16, p. 864.

[18] Tong T.W., Skocypec R.D., Summary on comparison of radiative heat transfer solutions for a specified problem, in: Proceedings of the 28th National Heat Transfer Conf., San Diego, CA, Vol. 203, American Society of Mechanical Engineers, New York, 1992, pp. 253–264.

[19] Tan Z.-M., Hsu P.-F., An integral formulation of transient radiative transfer, ASME J. Heat Tran. (2000) (accepted).

[20] Ozisik M.N., Radiative Transfer and Interaction with Conduction and Convection, Wiley, New York, 1973, chapter 8, p. 251.

[21] Modest M.F., Radiative Heat Transfer, McGraw-Hill, New York, 1993, chapter 8, p. 303.

[22] Tannehill J.C., Anderson D.A., Pletcher R.H., Computational Fluid Mechanics and Heat Transfer, 2nd ed., Taylor & Francis, Washington, DC, 1997.

[23] Fleck J.A., The calculation of nonlinear radiation transport by a Monte Carlo method, Methods Comput. Phys. 1 (1963) 43–65.